PAN
POLSKA AKADEMIA NAUK

M&MS

A NOVEL APPROACH TO DIAGNOSIS OF ANALOG CIRCUIT INCIPIENT FAULTS BASED ON KECA AND OAO LSSVM

Chaolong Zhang[1,2], Yigang He[1], Lei Zuo[1], Jinping Wang[1], Wei He[1]

1) Hefei University of Technology, School of Electrical Engineering and Automation, 230009 Hefei, China
(✉ zhangcl@aqtc.edu.cn, +86 551 6290 1408, 18655136887@163.com, benzl0313@126.com, waupter919@163.com, hfutwei@foxmail.com)
2) Anqing Normal University, School of Physics and Electronic Engineering, 246011 Anqing, China

Abstract

Correct incipient identification of an analog circuit fault is conducive to the health of the analog circuit, yet very difficult. In this paper, a novel approach to analog circuit incipient fault identification is presented. Time responses are acquired by sampling outputs of the circuits under test, and then the responses are decomposed by the wavelet transform in order to generate energy features. Afterwards, lower-dimensional features are produced through the kernel entropy component analysis as samples for training and testing a one-against-one least squares support vector machine. Simulations of the incipient fault diagnosis for a Sallen-Key band-pass filter and a two-stage four-op-amp bi-quad low-pass filter demonstrate the diagnosing procedure of the proposed approach, and also reveal that the proposed approach has higher diagnosis accuracy than the referenced methods.

Keywords: analog circuits, incipient fault diagnosis, wavelet transform, kernel entropy component analysis, least squares support vector machine.

1. Introduction

Generally, about 20% of an electronic system is analog, but about 80% of faults occur in this segment. The analog circuit fault diagnosis plays an important role in the preventive maintenance of electronic systems. Nevertheless, it falls far behind the well investigated digital circuit fault diagnosis, because of component tolerance effects, insufficient information, and nonlinearity of analog circuits.

During the recent few years, there has been useful research into the analog circuit fault diagnosis at board, system, and chip levels [1−16], [18, 19], [21−23]. The feature extraction and classifier selection are two main problems which need to be addressed in the analog circuit fault diagnosis. The feature extraction is the first problem, which strongly affects the successive classifier's efficiency. The effective features can reflect significant differences among fault classes, which contribute to a high-performance classifier. In the diagnosis performed in [2] impulse responses of the circuits under test (CUTs) were applied directly to the classifier, which caused a tremendous computing workload. The wavelet transform was introduced to the diagnosis [3−9], and coefficients [3−7] and coefficient energies [8, 9] were generated as features. The principal component analysis (PCA) [5], kernel principal component analysis (KPCA) [10], linear discriminant analysis (LDA) [11] and kernel linear discriminant analysis (KLDA) [12] were proposed to reduce the dimension of high-dimensional features for the purpose of simplifying the workload, and positive results were obtained. With regard to the successive classifier, an artificial neural network has been normally and widely used, for it can implement the fault diagnosis by using the extracted CUTs' performance data [13−16]. However, it has some disadvantages, as: failing to obtain

local optimal solution, a low convergence rate, and poor generalization. The support vector machine (SVM) [17] accounts for the trade-off between learning ability and generalizing ability by minimizing the structure risk, and has been used to the analog circuit fault diagnosis [18, 19]. The least squares support vector machine (LSSVM) enhances the SVM formulation by adopting a least-squares linear system as the loss function [20], which can reduce the computation complexity and improve the performance. Therefore, LSSVM is considered to be an effective tool for the analog circuit fault diagnosis in many recent works [21−23].

For the purpose of monitoring the performance degradation and predicting failures of analog circuits, it is very important to identify faults at their incipient stage. However, most of the above works focus on the analog circuit fault diagnosis, rather than the incipient fault diagnosis. The reason is that overlapping different fault classes easily occurs, since a difference between incipient fault and nominal values of each component is small, which makes distinguishing various incipient fault classes difficult.

The Kernel entropy component analysis (KECA) is a spectral method based on a kernel similarity matrix and manages to maintain the maximum Renyi entropy of input space data set [24]. In this paper, a novel approach for the analog circuit incipient fault diagnosis based on KECA and one-against-one (OAO) LSSVM is presented. The wavelet transform is employed to process the measured impulse signals to produce energy features. KECA is used to reduce the dimension of energy features and to generate low-dimensional features as input data. Different incipient fault classes are classified by OAO LSSVM. Incipient fault diagnosis simulations of a Sallen-Key band-pass filter and two-stage four-op-amp bi-quad low-pass filter circuit have been carried out to demonstrate the proposed approach. In addition, KECA has been compared with KPCA in visualization effect of scatter plots, and also compared with PCA, KPCA and KLDA in the diagnosis simulation.

The material in the paper is organized in the following order: Section 2 briefly describes the wavelet transform and generation of energy features. Section 3 introduces KECA. OAO LSSVM is presented in Section 4. Section 5 shows simulation results and their discussion. Finally, Section 6 contains the conclusions.

2. Wavelet transform and generation of features

The wavelet transform is an effective technique which has been widely used in signal processing [25]. It decomposes a signal $f(x)$ into details and approximations.

Let us assume that $\psi(x)$ is a mother wavelet defined as:

$$\psi_{a,b}(x) = \frac{1}{\sqrt{a}} \psi(\frac{x-b}{a}), \tag{1}$$

where a is the scaling parameter and b is the translating parameter.

The wavelet transform of $f(x)$ is:

$$c(a,b) = \langle f(x), \psi_{a,b}(x) \rangle = \frac{1}{\sqrt{a}} \int_{-\infty}^{+\infty} f(x)\psi(\frac{x-b}{a}), \tag{2}$$

where $c(a, b)$ refer to the wavelet coefficients of $f(x)$.

Let us assume that Z is a set of integers; $\{V_k\}_{k \in Z}$ is the orthogonal multi-resolution analysis; $\{W_k\}_{k \in Z}$ is the associated wavelet space. The $f(x)$ projection on V_k can be obtained by:

$$P_{V_k} f = P_{V_{k+1}} f + P_{W_{k+1}} f = \sum_{i \in Z} c_{k+1}^i \phi_{k+1,i} + \sum_{i \in Z} d_{k+1}^i \psi_{k+1,i}, \tag{3}$$

where $P_{V_{k+1}}f$ and $P_{W_{k+1}}f$ refer to the $f(x)$ projections on V_{k+1} and W_{k+1} at 2^{k+1} resolution, respectively; c^i_{k+1} and d^i_{k+1} denote the scaling and wavelet coefficients of $f(x)$ at 2^{k+1} resolution, respectively; ϕ_{k+1} and ψ_{k+1} refer to the scaling and wavelet functions at 2^{k+1} resolution, respectively. Therefore, c_{k+1} and d_{k+1} represent the approximations and details which are the low-frequency and high-frequency components of $f(x)$ at 2^{k+1} resolution, respectively. Correspondingly, $\{V_k\}_{k\in Z}$ can be decomposed as:

$$
\begin{aligned}
V_k &= W_{k+1} \oplus V_{k+1} = W_{k+1} \oplus (W_{k+2} \oplus V_{k+2}) \\
&= W_{k+1} \oplus W_{k+2} \oplus (W_{k+3} \oplus V_{k+3}) \\
&= W_{k+1} \oplus W_{k+2} \oplus W_{k+3} \oplus \cdots .
\end{aligned}
\tag{4}
$$

The detail and approximation coefficients can be obtained from (3) and (4). Since the approximation coefficients can capture the basic structure of the signal $f(x)$, the coefficient energies at various levels are obtained:

$$
E_{k+1} = \sum_{i=1}^{u} | c^i_{k+1} |^2 ,
\tag{5}
$$

where $i = 1,2,\ldots u$ and u is the length of low-frequency component at 2^{k+1} resolution. For the sake of avoiding large dynamic ranges in one or more dimensions, the energies of detail coefficients at various levels are normalized, and then the energy features are generated. The Haar function has a regularity of zero and a compact support, so it is well suitable to extract features from signals characterized by swift variations and short durations. Hence, the Haar wavelet is used as the wavelet function in the work.

3. KECA

In order to simplify the workload, a dimension reduction approach needs to be used to reduce the dimension of energy features. Compared to the widely used KPCA [26], KECA is a novel technique in the dimension reduction field [27, 28]. It manages to maintain the maximum Renyi entropy of input space data set, and in contrast to KPCA maintains second-order statistics of data set maximally. Hence, KECA is employed to perform dimension reduction in the work.

The Renyi quadratic entropy is defined as:

$$
H(p) = -\log \int p^2(x)d\,x ,
\tag{6}
$$

where $p(x)$ is the probability density function. Since logarithm is a monotonic function, the quantity is defined as:

$$
V(p) = \int p^2(x)d\,x .
\tag{7}
$$

A Parzen window density estimator is deduced in order to estimate $V(p)$ and $H(p)$:

$$
\hat{p}(x) = \frac{1}{N} \sum_{x_u \in D} k_\sigma(x, x_u) ,
\tag{8}
$$

where $k_\sigma(x, x_u)$ is the Parzen window and $D = x_1, x_2,\ldots, x_N$.

The sample mean approximation of the expectation operator is used:

$$\hat{V}(p) = \frac{1}{N} \sum_{\mathbf{x}_u \in D} \hat{p}(\mathbf{x}_u) = \frac{1}{N} \sum_{\mathbf{x}_u \in D} \frac{1}{N} \sum_{\mathbf{x}_{u'} \in D} k_\sigma(\mathbf{x}_u, \mathbf{x}_{u'})$$
$$= \frac{1}{N^2} \mathbf{C}^\mathrm{T} \mathbf{K} \mathbf{C}, \tag{9}$$

where $\mathbf{C}$ is an $N \times 1$ vector of ones and $\mathbf{K}$ is an $N \times N$ kernel matrix which elements (u, u') are equal to $k_\sigma(\mathbf{x}_u, \mathbf{x}_{u'})$. On the basis of eigenvalues and eigenvectors of the kernel matrix, $\mathbf{K}$ is eigen-decomposed as:

$$\mathbf{K} = \mathbf{E} \mathbf{A}_\mu \mathbf{E}^\mathrm{T}, \tag{10}$$

where $\mathbf{E}$ is a matrix which columns are the eigenvectors $\mathbf{e}_1, \mathbf{e}_2, \cdots, \mathbf{e}_N$ and $\mathbf{A}_\mu$ is a diagonal matrix which elements are the eigenvalues. $\hat{V}(p)$ can be expressed as:

$$\hat{V}(p) = \frac{1}{N^2} \sum_{i=1}^{N} (\sqrt{\mu_i} \mathbf{e}_i^\mathrm{T} \mathbf{C})^2 = \frac{1}{N^2} \sum_{i=1}^{N} \lambda_i. \tag{11}$$

Each term $\lambda_i = (\sqrt{\mu_i} \mathbf{e}_i^\mathrm{T} \mathbf{C})^2$ contributes to the entropy estimate in the expression (11). The first h largest contribution eigenvalues and eigenvectors are selected, then $\phi_{eca} = \mathbf{A}_h^{1/2} \mathbf{E}_h^\mathrm{T}$, and $\mathbf{K}_{eca} = \phi_{eca}^\mathrm{T} \phi_{eca}$ can be acquired in the Mercer kernel space. This is the primary difference between KECA and KPCA.

4. LSSVM

LSSVM is an improvement of the standard SVM. In the algorithm, a quadratic programming problem is replaced by a linear set of equations to obtain the support vectors and a least-squares linear system is adopted as the loss function. A model is defined in the primal weight space:

$$y(\mathbf{x}) = w^\mathrm{T} \varphi(\mathbf{x}) + b, \tag{12}$$

where $\mathbf{x}_i \in R^N$ and $y_i \in R$ are input and output, respectively; b is bias; w is an element of R^N; $\varphi(\cdot)$ is in charge of mapping the input data to a high dimensional feature space. Considering the functional complexity and fitting error, the LSSVM optimization problem can be defined as:

$$\min_{w, b, \xi} \frac{1}{2} w^\mathrm{T} w + \frac{1}{2} c \sum_{i=1}^{l} \xi_i^2, \tag{13}$$

$$\mathrm{s.t.}: \xi_i = y_i - [w^\mathrm{T} \phi(\mathbf{x}_i) + b] \quad \forall i = 1, 2, \ldots, l, \tag{14}$$

where c and ξ_i are the penalty parameter and random errors, respectively.

The Lagrangian of (13) is given by:

$$L(w, b, \xi, a) = \frac{1}{2} w^\mathrm{T} w + \frac{1}{2} c \sum_{i=1}^{l} \xi_i^2 - \sum_{i=1}^{l} a_i \{ y_i - [w^\mathrm{T} \phi(\mathbf{x}_i) + b] - \xi_i \}, \tag{15}$$

where α_i are Lagrange multipliers. The solution of (15) can be obtained by partially differentiating in regard to each variable:

$$\begin{cases} \dfrac{\partial L}{\partial w} = 0 \Rightarrow w = \sum_{i=1}^{l} a_i \phi(\mathrm{x}_i) \\[2mm] \dfrac{\partial L}{\partial b} = 0 \Rightarrow \sum_{i=1}^{l} a_i = 0 \\[2mm] \dfrac{\partial L}{\partial \xi_i} = 0 \Rightarrow a_i = c\xi_i \quad \forall i = 1,2,\ldots l \\[2mm] \dfrac{\partial L}{\partial a_i} = 0 \Rightarrow \xi_i = y_i - [w^{\mathrm{T}}\phi(\mathrm{x}_i) + b] \quad \forall i = 1,2,\ldots l. \end{cases} \tag{16}$$

After variables w and ξ_i are eliminated, the equation can be substituted as a linear function group:

$$\begin{pmatrix} K + c^{-1}I & \vec{1}^{\mathrm{T}} \\ \vec{1} & 0 \end{pmatrix} \begin{pmatrix} a \\ b \end{pmatrix} = \begin{pmatrix} Y \\ 0 \end{pmatrix}, \tag{17}$$

where $\alpha = [\alpha_1, \ldots, \alpha_l]^{\mathrm{T}}$; $Y = [y_1, \ldots, y_l]^{\mathrm{T}}$; $K_{ij} = k(\mathrm{x}_i, \mathrm{x}_j)$, and is a kernel function which follows the Mercer's theory; $\vec{1} = [1, \ldots, 1]$.

The LSSVM model can be described as:

$$y(\mathrm{x}) = \sum_{i=1}^{l} a_i k(\mathrm{x}_i, \mathrm{x}_j) + b, \tag{18}$$

where a_i and b are solutions to the linear system.

LSSVM is originally designed as a binary classifier, but the analog circuit incipient fault diagnosis is a multi-class recognition problem. Hence, a one-against-one (OAO) LSSVM is selected to address the m-class problem in analog circuit fault diagnosis. OAO LSSVM needs to constitute $m*(m-1)/2$ binary LSSVM classifiers, and each classifier is trained using the data of one class as positive and the data of another class as negative. Max Wins algorithm is adopted to combine these results of classifiers and it explores the resultant class of the input data by choosing the class voted by the majority of LSSVM classifiers.

5. Simulations and results

The occurrence probability of a single incipient fault condition is significantly higher than a multiple incipient fault condition in the analog circuit incipient fault diagnosis, and the approach which is available for a single fault condition can also be applied to a multiple fault condition. Hence, the single incipient fault condition is taken for granted to demonstrate the proposed diagnosis approach.

5.1. Simulation procedure and settings

In this section, a Sallen-Key band-pass filter with 25 kHz central frequency and a two-stage four-op-amp bi-quad low-pass filter with 10 kHz central frequency are considered as exemplary circuits. A single 10 V pulse with 10 us duration is used as the input. Time responses are acquired by sampling the CUTs' outputs. Let us assume the tolerances of resistors and capacitors are 5%. Generally, a component is considered to be faulty when its value has deviated from its nominal value by about 50% [2−16], [18, 19], [21−23], therefore a component with a 25% deviation from its nominal value is considered to indicate an incipient fault in the work. 100 output sample data for each fault class have been collected. Combining

effectiveness and efficiency, the 6-level Haar wavelet transform has been employed to decompose the time responses for the purpose of generating 6-dimensional energy features. Furthermore, the lower-dimensional data have been obtained as samples through KECA. For the sake of convenience and simplicity in visualization and comparison, the original 6-dimensional features are reduced to 2-dimensional features. The first 50 sample data have been used to train OAO LSSVM to set up a classification model, whereas the rest 50 sample data have been applied to test the performance of the classification model. The simulation procedure is shown in Fig. 1.
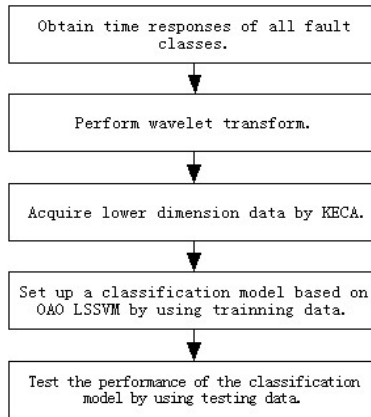
Fig. 1. The simulation procedure.

5.2. Simulation results and analysis

5.2.1. Example 1 − Sallen-Key band-pass filter

A Sallen-Key band-pass filter circuit showed in Fig. 2 is used as the first exemplary circuit. The nominal value of each component is labeled in the figure. Through the component sensitivity analysis, R2, R3, C1 and C2 are considered to be the critical components, since they have a greater impact on the center frequency. Hence, the components are selected as experiment components. The faulty impulse responses are processed so as to form 9 fault classes, including R2↑, R2↓, R3↑, R3↓, C1↑, C1↓, C2↑, C2↓ and no fault (NF), where ↑ and ↓ refer to values higher and lower than the nominal one, respectively. The fault codes, fault classes, nominal and faulty component values are shown in Table 1.
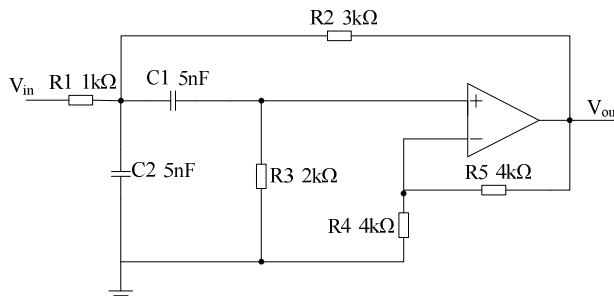

Fig. 2. The Sallen-Key band-pass filter circuit.

Table 1. The fault codes, fault classes, nominal and faulty component values for band-pass filter.

Fault code	Fault class	Nominal	Faulty value
F0	NF	–	–
F1	R2↑	3kΩ	3.75kΩ
F2	R2↓	3kΩ	2.25kΩ
F3	R3↑	2kΩ	2.5kΩ
F4	R3↓	2kΩ	1.5kΩ
F5	C1↑	5nF	6.25nF
F6	C1↓	5nF	3.75nF
F7	C2↑	5nF	6.25nF
F8	C2↓	5nF	3.75nF
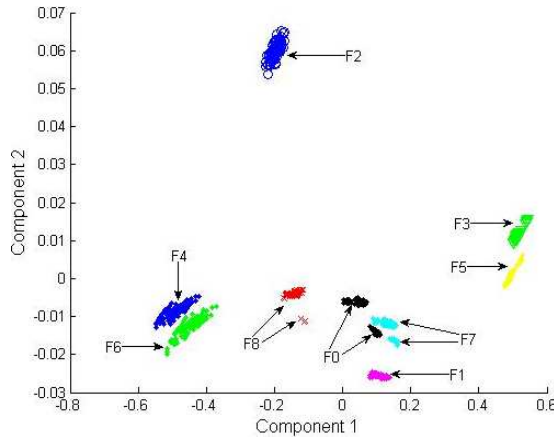
Fig. 3. The scatter plots of fault classes characterized by 2-dimensional features of band-pass filter by KECA.
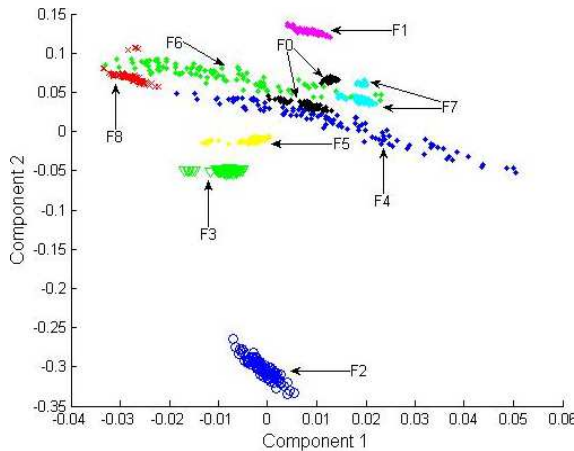

Fig. 4. The scatter plots of fault classes characterized by 2-dimensional features of band-pass filter by KPCA.

Subsequently, the first two most significant component vectors which contribute the most to the Renyi entropy are extracted by KECA. Fig. 3 reveals the scatter plots of fault classes characterized by 2-dimensional features. It is obvious that F0, F1, F2, F3, F4, F5, F6, F7 and F8 fault classes are distinct ambiguity groups. This manifests all fault classes are well separated by KECA. This is conducive to the classifications of OAO LSSVM. The first 50 sample data from each fault class group have been randomly selected as training data in order

to train OAO LSSVM, and the rest 50 sample data have been used to test. The overall diagnosis accuracy in the simulation is 100%.

In order to make a visualization comparison, KPCA is applied to reduce the dimension of the energy features. The first two principal component vectors with the first two large eigenvalues have been generated and the reduced 2-dimensional features are shown in Fig. 4. It is obvious that F1, F2, F3, F4 and F5 fault classes are distinct ambiguity groups in the figure. However, there is obvious overlapping for F0, F6, F7 and F8 fault classes. It can be observed from Figs. 3 and 4 that the KECA based groups of samples are clearer and much better from the classification point of view when compared to KPCA. This reveals that KECA can generate better extraction performance than KPCA.

5.2.2. Example 2 − Two-stage four-op-amp bi-quad low-pass filter

A two-stage four-op-amp bi-quad low-pass filter is shown in Fig. 5, and it is used as another exemplary circuit. The circuit is more complex, since it consists of 4 capacitors, 24 resistors and 8 operational amplifiers. Each component value has been labeled in the figure. R4, R6, R7, R9, R18, C2 and C4 have been selected as the experiment components. 15 fault classes, including R4↑, R4↓, R6↑, R6↓, R7↑, R7↓, R9↑, R9↓, R18↑, R18↓, C2↑, C2↓, C4↑, C4↓ and NF, have been formed after the faulty impulse responses were processed. The fault codes, fault classes, nominal and faulty component values are shown in Table 2.
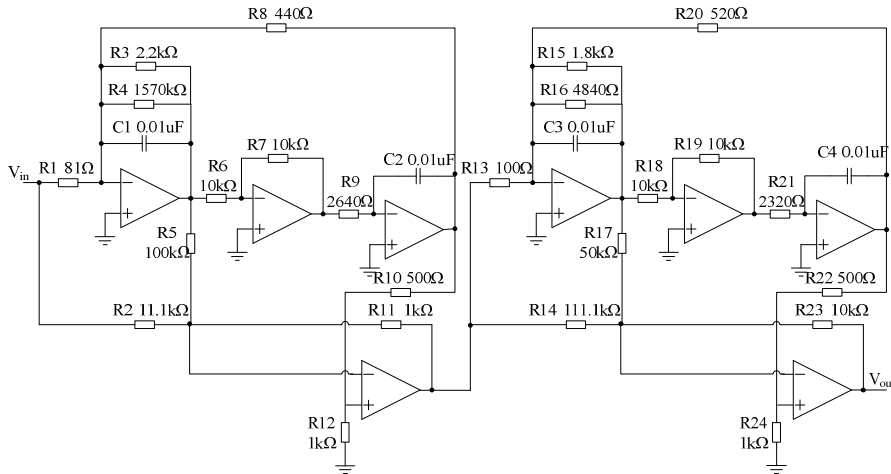

Fig. 5. The two-stage four-op-amp bi-quad low-pass filter circuit.

After acquiring the energy features, KECA is used to reduce the dimension of energy features to 2. Fig. 6 reveals the scatter plots of fault classes characterized by 2-dimensional features. It is obvious that F1, F4, F5, F6, F8, F10, F12 and F14 fault classes are distinct ambiguity groups, whereas F3, F7 and F11 fault classes are partially overlapping. However, it is difficult to distinguish whether F9 and F13 fault classes, as well as F0 and F2 fault classes are overlapping in the figure. Therefore, the scatter plots of F9, F13 and other fault classes, F0, F2 and other fault classes are magnified and shown in Fig. 7a and Fig. 7b, respectively. It is obvious that F0, F2, F9 and F13 fault classes are non-overlapping in the figure. Fig. 8 shows the scatter plots of fault classes characterized by 2-dimensional features by KPCA. F0, F1, F2, F4, F5, F6, F8, F9, F12, F13 and F14 fault classes are distinct ambiguity groups in the figure. Nevertheless, there is complete overlapping for F3, F7, F10 and F11 fault classes. This

example also reveals that KECA can generate better extraction performance than KPCA.

Table 2. The fault codes, fault classes, nominal and faulty component values for low-pass filter.

Fault code	Fault class	Nominal	Faulty value
F0	NF	–	–
F1	R4↑	1570Ω	1962Ω
F2	R4↓	1570Ω	1176Ω
F3	R6↑	10kΩ	12.5kΩ
F4	R6↓	10kΩ	7.5kΩ
F5	R7↑	10kΩ	12.5kΩ
F6	R7↓	10kΩ	7.5kΩ
F7	R9↑	2640Ω	3300Ω
F8	R9↓	2640Ω	1980Ω
F9	R18↑	10kΩ	12.5kΩ
F10	R18↓	10kΩ	7.5kΩ
F11	C2↑	0.01nF	0.0125nF
F12	C2↓	0.01nF	0.0075nF
F13	C4↑	0.01nF	0.0125nF
F14	C4↓	0.01nF	0.0075nF

Based on the visualization effect of scatter plots in Figs. 3, 4, 6, 7 and 8, it can be easily learned that the separability of features reduced by KECA is further enlarged than by KPCA, and this indicates that different fault classes can be well separated by KECA. Therefore, choosing significant components based on Renyi entropy is more appropriate in the analog circuit incipient fault diagnosis. Meanwhile, the faults processed by KECA can be identified more conveniently and satisfactorily than by KPCA.
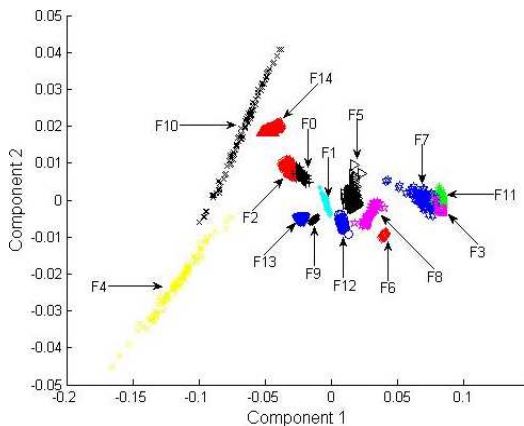

Fig. 6. The scatter plots of fault classes characterized by 2-dimensional features of low-pass filter by KECA.

The first 50 sample data and the rest 50 sample data of each fault class have been used as training data and testing data, respectively. Table 3 demonstrates accuracies of the diagnosis approach in diagnosing the 15 fault classes. The F0, F1, F2, F4, F5, F6, F8, F9, F10, F12, F13 and F14 fault classes can be classified correctly. Meanwhile, 50 test data of the F3 fault class are classified correctly 49 times and misclassified as the F7 fault class once; 50 test data of the F7 fault class are classified correctly 46 times, and misclassified as the F3 fault class twice and the F11 fault class twice; 50 test data of the F11 fault class are classified correctly 45 times, and misclassified as the F3 fault class twice and the F7 fault class 3 times. The overall diagnosis accuracy is 98.7%.
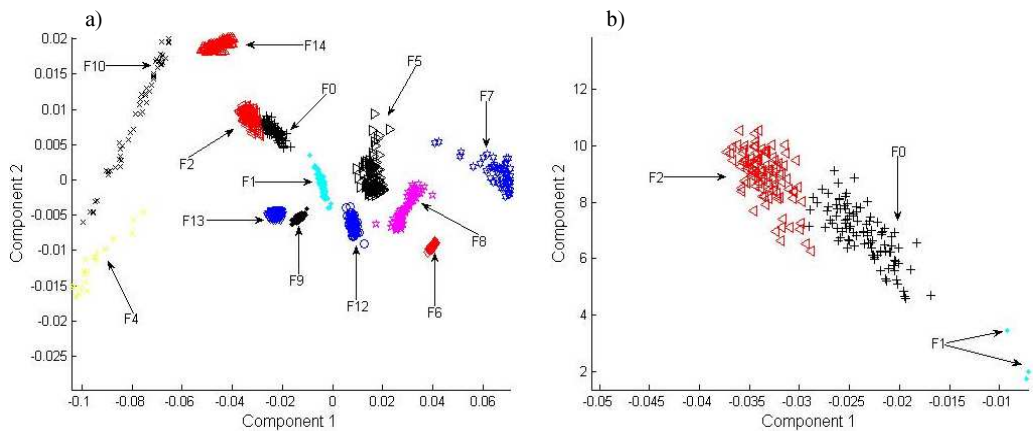
Fig.7. The scatter plots of a) F9, F13 and other fault classes and b) F0, F2 and other fault classes characterized by 2-dimensional features of low-pass filter by KECA.
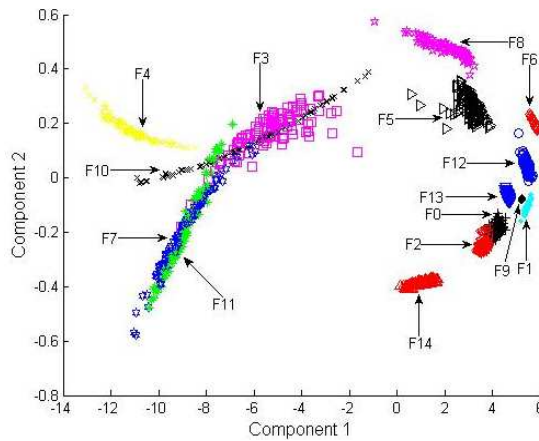

Fig. 8. The scatter plots of fault classes characterized by 2-dimensional features of low-pass filter by KPCA.

Table 3. Accuracies of the diagnosis approach for low-pass filter.

Fault code	Fault class	Accuracy
F0	NF	100%
F1	R4↑	100%
F2	R4↓	100%
F3	R6↑	98%
F4	R6↓	100%
F5	R7↑	100%
F6	R7↓	100%
F7	R9↑	92%
F8	R9↓	100%
F9	R18↑	100%
F10	R18↓	100%
F11	C2↑	90%
F12	C2↓	100%
F13	C4↑	100%
F14	C4↓	100%

5.3. Comparison of simulation results

PCA [5], improved KPCA [10] and KLDA [12] have been used to reduce the dimension of features in recent analog circuit fault diagnosis works [5, 10, 12]. The proposed diagnosis approach in our work is compared with the approaches in [5, 10, 12]. The energy features of example 1 and example 2 are used to test the referenced approaches and compare the simulation results for performed incipient fault diagnoses under the same simulation conditions. The diagnosis accuracy of each approach is shown in Table 4. From the results contained in the table, it can be observed that performing the incipient fault diagnosis by using KLDA as a preprocessor allows to obtain more positive results than by using PCA and KPCA. Meanwhile, the results in the last column show that the proposed approach has higher diagnosis accuracy than the referenced approaches.

Table 4. The diagnosis accuracies of our approach and the referenced approaches.

Example	Reference [5]	Reference [10]	Reference [12]	Our work
Example 1-bandpass filter	97.1%	99.1%	99.6%	100%
Example 2-lowpass filter	95.9%	97.9%	98.4%	98.7 %

6. Conclusions

In this work, a novel approach has been presented to perform the analog circuit incipient fault diagnosis by using the wavelet transform, KECA and OAO LSSVM. The wavelet transform of time responses has produced coefficients at various levels and further generated the energy features which are related to each of fault classes. KECA has been used to reduce the dimension of energy features from a high dimension to a low dimension. Different fault classes have been identified by OAO LSSVM. Through comparing the scatter plots of fault classes characterized by 2-dimensional features, it can be easily concluded that KECA is better than KPCA in dimension reduction. Comparison of simulation results have verified that the proposed approach has higher diagnosis accuracy than the referenced methods.

Acknowledgements

References

[1] Pułka, A. (2011). Two heuristic algorithms for test point selection in analog circuit diagnoses. *Metrol. Meas. Syst.*, 18(1), 115–128.

[2] Spina, R., Upadhyaya, S. (1997). Linear circuit fault diagnosis using neuromorphic analyzers. *IEEE Trans. Circuits Syst. II, Analog Digit. Signal Process.*, 44(3), 188–196.

[3] Aminian, F., Aminian, M. (2001). Fault diagnosis of analog circuits using Bayesian neural networks with wavelet transform as preprocessor. *J. Electron. Test.*, 17(1), 29–36.

[4] Aminian, M., Aminian, F. (2007). A modular fault-diagnostic system for analog electronic circuits using neural networks with wavelet transform as a preprocessor. *IEEE Trans. Instrum. Meas.*, 56(5), 1546–1554.

[5] Xiao, Y., He, Y. (2010). A linear ridgelet network approach for fault diagnosis of analog circuit. *Sci. China Inf. Sci.*, 53(11), 2251–2264.

[6] Aminian, M, Aminian, F. (2000). Neural-network based analog-circuit fault diagnosis using wavelet transform as preprocessor. *IEEE Trans. Circuits Syst. II, Analog Digit. Signal Process.*, 47(2), 151–156.

[7] Aminian, F., Aminian, M., Collins, H.W. (2002). Analog fault diagnosis of actual circuits using neural networks. *IEEE Trans. Instrum. Meas.*, 51(3), 544–550.

[8] He, Y., Tan, Y., Sun, Y. (2004). Wavelet neural network approach for fault diagnosis of analogue circuits. *Proc. Inst. Elect. Eng. − Circuits, Devices Syst.*, 151(4), 379–384.

[9] Long, B., Huang, J., Tian, S. (2008). Least squares support vector machine based analog-circuit fault diagnosis using wavelet transform as pre-processor. *ICCCAS 2008.*, 1026–1029.

[10] Xiao, Y., He, Y. (2011). A novel approach for analog fault diagnosis based on neural networks and improved kernel PCA. *Neurocomputing*, 74(7), 1102–1115.

[11] Xu, L., Huang, J., Wang, H., Long, B. (2010). A novel method for the diagnosis of the incipient faults in analog circuits based on LDA and HMM. *Circuits Syst. Signal Process.*, 29(4), 577–600.

[12] Xiao, Y., Feng, L. (2012). A novel neural-network approach of analog fault diagnosis based on kernel discriminant analysis and particle swarm optimization. *Appl. Soft. Comput.*, 12(2), 904–920.

[13] Yuan, L., He, Y., Huang, J., Sun, Y. (2010). A new neural-network-based fault diagnosis approach for analog circuits by using kurtosis and entropy as a preprocessor. *IEEE Trans. Instrum. Meas.*, 59(3), 586–595.

[14] Toczek, W., Kowalewski, M. (2005). A neural network based system for soft fault diagnosis in electronic circuits. *Metrol. Meas. Syst.*, 12(4), 463–476.

[15] Grzechca, D. (2011). Soft fault clustering in analog electronic circuits with the use of self organizing neural network. *Metrol. Meas. Syst.*, 18(4), 555–568.

[16] Tan, Y., He, Y., Cui, C., Qiu, G. (2008). A novel method for analog fault diagnosis based on neural networks and genetic algorithms. *IEEE Trans. Instrum. Meas.*, 57(11), 2631–2639.

[17] Cortes, C., Vapnik, V. (1995). Support-vector networks. *Mach Learn.*, 20(3), 273–297.

[18] Grzechca, D., Rutkowski, J. (2009). Fault diagnosis in analog electronic circuits-the SVM approach. *Metrol. Meas. Syst.*, 16(4), 583–598.

[19] Cui, J., Wang, Y. (2010). A novel approach of analog fault classification using a support vector machines classifier. *Metrol. Meas. Syst.*, 17(4), 561–581.

[20] Suykens, J.A.K., Vandewalle, J. (1999). Least squares support vector machine classifiers. *Neural Process Lett.*, 9(3), 293–300.

[21] Vasan, A.S.S., Long, B., Pecht, M. (2013). Diagnostics and prognostics method for analog electronic circuits. *IEEE TInd Electron.*, 60(11), 5277–5291.

[22] Cui, J., Wang, Y. (2011). Analog circuit fault classification using improved one-against-one Support Vector Machines. *Metrol. Meas. Syst.*, 18(4), 569–582.

[23] Long, B., Tian, S., Wang, H. (2012). Feature vector selection method using Mahalanobis distance for diagnostics of analog circuits based on LS-SVM. *J. Electron. Test.*, 28(5), 745–755.

[24] Jenssen, R. (2010). Kernel entropy component analysis. *IEEE T. Pattern. Anal.*, 32(5), 847–860.

[25] Arizmendi, C., Vellido, A., Romero, E. (2012). Classification of human brain tumours from MRS data using Discrete Wavelet Transform and Bayesian Neural Networks. *Expert Syst. Appl.*, 39(5), 5223–5232.

[26] Ni, J., Zhang, C., Yang, S.X. (2011).An adaptive approach based on KPCA and SVM for real-time fault diagnosis of HVCBs. *IEEE T. Power Deliver.*, 26(3), 1960–1971.

[27] Shekar, B.H., Sharmila, K.M., Mestetskiy L.M., Dyshkantc, N.F. (2011). Face recognition using kernel entropy component analysis. *Neurocomputing*, 74(6), 1053–1057.

[28] Gomez-Chova, L., Jenssen, R., Camps-Valls, G. (2012). Kernel Entropy Component Analysis for Remote Sensing Image Clustering. *IEEE Geosci Remote S.*, 9(2), 312–316.